Editors' Suggestion

Coherent and Incoherent Tunneling into Yu-Shiba-Rusinov States Revealed by Atomic Scale Shot-Noise Spectroscopy

U. Thupakula,[1] V. Perrin,[1] A. Palacio-Morales,[1] L. Cario,[2] M. Aprili,[1] P. Simon,[1] and F. Massee[1,*]

[1]*Laboratoire de Physique des Solides (CNRS UMR 8502), Bâtiment 510, Université Paris-Sud/Université Paris-Saclay, 91405 Orsay, France*

[2]*Université de Nantes, CNRS, Institut des Matériaux Jean Rouxel, IMN, F-44000 Nantes, France*

(Received 26 October 2021; revised 27 December 2021; accepted 18 May 2022; published 15 June 2022)

The pair breaking potential of individual magnetic impurities in *s*-wave superconductors generates localized states inside the superconducting gap commonly referred to as Yu-Shiba-Rusinov (YSR) states whose isolated nature makes them promising building blocks for artificial structures that may host Majorana fermions. One of the challenges in this endeavor is to understand their intrinsic lifetime, $\hbar/\Lambda$, which is expected to be limited by the inelastic coupling with the continuum thus leading to decoherence. Here we use shot-noise scanning tunneling microscopy to reveal that electron tunneling into superconducting 2H-$NbSe_2$ mediated by YSR states is not Poissonian, but ordered as a function of time, as evidenced by a reduction of the noise. Moreover, our data show the concomitant transfer of charges e and $2e$, indicating that incoherent single particle and coherent Andreev processes operate simultaneously. From the quantitative agreement between experiment and theory we obtain $\Lambda = 1\ \mu\text{eV} \ll k_B T$ demonstrating that shot noise can probe energy scales and timescales inaccessible by conventional spectroscopy whose resolution is thermally limited.

DOI: 10.1103/PhysRevLett.128.247001

Introduction.—For a single impurity spin in a superconductor, a bound state appears inside the gap [1–3] with its particle and hole components located in energy symmetrically around zero [4]. The amplitudes of the two components are usually different [5–7] and reflect the coherence factors of the electron and hole excitations. Whereas the spatial extent of the YSR states is typically on the order of a few atoms [5], they have been shown to range up to tens of nanometers for two-dimensional superconductors [8]. Since the YSR states are inside the superconducting gap, one of the key questions, particularly with an eye on building more complicated structures such as chains and islands [9–12], is how electrons relax from the YSR states into the condensate. Not only is a full understanding of the nature of the impurity and its intrinsic lifetime important for theoretical modeling, the dynamics of charge transfer through it can, in principle, also be used to directly distinguish conventional YSR states from Majorana bound states [13].

The high spatial and energy resolution make the scanning tunneling microscope (STM) an ideal experimental tool to investigate the tunneling process into individual impurities. Previous studies using the time averaged current and theoretical modeling showed tantalizing signatures of a transition from single-electron dominated tunneling to multiparticle Andreev processes [14,15]. Direct evidence for such a transition, and more specifically for Andreev processes to occur with a standard metallic probe, however, is lacking. Moreover, direct tunneling into the magnetic impurity can complicate the interpretation of the data, since the impurity state may be affected by the presence of the tip [17–20], or multiple tunneling paths and relaxation processes may occur [21–23], which are difficult to incorporate in theory.

Although experimentally challenging, atomic scale shot-noise measurements can, in principle, resolve all these issues. This is because shot noise (S_{shot}), which is current noise originating from the discreteness of the charge carriers, is sensitive to both the charge of the carriers q, as well as the nature of the tunneling process [24]. To evaluate the shot noise, we consider the effective Fano factor, $F^* = S_{\text{shot}}/2e|I| = qF/e$, where I is the time averaged current, e the electron charge, and F the Fano factor. For uncorrelated elastic quasiparticle tunneling between a metallic tip and the bulk superconductor, the electrons follow Poissonian statistics [25] giving $F^* = F = 1$ [EQP in Fig. 1(a)]. Single electron tunneling via the YSR states, on the other hand, is a resonant process and only possible through inelastic quasiparticle relaxation. Therefore, the electron flow will become ordered, thereby reducing the current noise from Poissonian to sub-Poissonian, i.e., $F^* < 1$ [IQP in Fig. 1(a)], as observed in quantum dots [26]. Alternatively, Andreev reflection through the YSR state transfers a charge of $q = 2e$, giving $F^* > 1$ [AR in Fig. 1(a)], enabling them to be easily distinguished from either form of single electron tunneling [25,27,28].

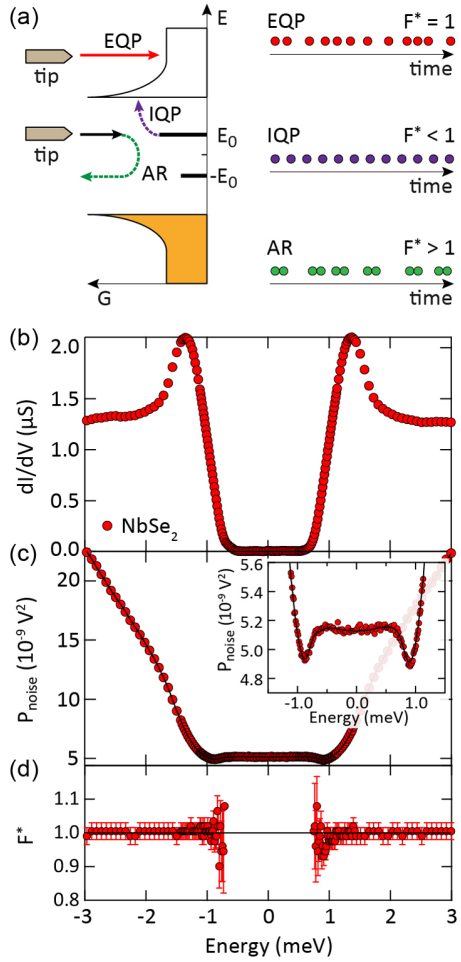

FIG. 1. (a) Schematic depiction of the various tunneling processes into 2H-$NbSe_2$: direct elastic quasiparticle tunneling into the bulk (EQP, red) inelastic quasiparticle tunneling through the YSR state (IQP, purple) and Andreev reflection assisted by the YSR (AR, green). The right panels illustrate the passage of electrons as a function of time: random, ordered, or in pairs, respectively. (b) Differential conductance of fully gapped 2H-$NbSe_2$, setup conditions: $V = 3$ mV, $I = 3$ nA. The sample is cleaved *in situ* at ~20 K and directly inserted in the STM head held at 4.2 K. All data throughout this Letter are recorded at $T = 0.3$ K (effective electron temperature ~0.7 K, see [30]) with an etched W tip. (c) Current noise power recorded simultaneously with (b), the black line is a fit for $F^* = 1$. The inset highlights the effect of the strongly varying dynamical resistance on the measured voltage noise that is accurately captured by the fit. (d) Effective Fano factor for the data in (c) giving $F^* = 1$ within error bars for all voltages. Data for currents < 10 pA are omitted for clarity.

Results.—Noise at the atomic scale is measured using our home-built scanning tunneling microscope with cryogenic circuitry operating in the MHz regime [29]. The circuitry (see Supplemental Material [30], Sec. 1 for more details) converts the current noise of the junction into voltage noise at the input of a cryogenic amplifier and operates simultaneously with conventional low frequency (dc) measurements. With sufficient averaging, the high stability and low temperature of our setup then allow us to resolve the shot-noise power produced by a tunneling current as small as 10 pA. Importantly for this Letter, when the junction resistance becomes comparable to the input impedance of the amplifier, part of the current noise is shorted by the junction itself. For a highly nonlinear $I(V)$ characteristic, such as that of clean 2H-$NbSe_2$ [Fig. 1(b)], one thus needs to take into account the dynamical resistance, $R_J(V) = dV/dI$, when analyzing the measured voltage noise. Figure 1(c) shows this effect vividly: instead of a simple linear current dependence of the measured noise power, it decreases at the onset of the coherence peak ($\sim \pm 0.9$ mV) below that obtained at zero voltage. This is because the reduced $R_J(V)$ at the coherence peaks lowers the contribution of the thermal noise more than that of the shot noise increases. Once the dynamical resistance is properly taken into account (see Ref. [30], Sec. 1C) we obtain $F^* = 1$ for all voltages where the current is large enough to detect shot noise accurately [Fig. 1(d)] as expected for quasiparticle tunneling following Poissonian statistics [25] [EQP in Fig. 1(a)].

Two YSR states with opposite particle-hole asymmetry, as well as a different spatial extent and YSR-to-coherence peak ratio are shown in Fig. 2 [38]. To evaluate their respective in-gap noise shown in Figs. 2(d) and 2(i), we fit the normal state ($|V| > 1.2$ mV) noise data using the measured $R_J(V)$ and $F^* = 1$, then extend the fit inside the gap. Unlike for clean 2H-$NbSe_2$ [Fig. 1(c)], the noise on the YSR cores does not follow $F^* = 1$: for the dominant resonance, i.e., positive bias for Figs. 2(c) and 2(d) and negative bias for Figs. 2(h) and 2(i), the noise is reduced ($F^* < 1$), whereas for the weak resonance it is enhanced ($F^* > 1$). Although the deviations in absolute numbers are relatively small, they correspond to changes in F^* of the order of 10% [Figs. 2(e) and 2(j)]. Importantly, the observation of $F^* > 1$ strongly suggests Andreev processes to be present, as it cannot occur for single electron tunneling into a one-level system. Furthermore, the reduced noise at opposite polarity also suggests a contribution from single electron tunneling, meaning both processes operate simultaneously.

To make a more quantitative analysis of the noise, and in order to avoid possible mechanical instabilities [17–20], multipath tunneling processes [21–23], or current-driven spin flip of the impurity [41] due to direct tunneling into the impurity, we shift our attention to the YSR tails where direct tunneling into the core is negligible. Since the particle-hole asymmetry of the tails oscillates as a function of distance from the core [8], we can probe locations where the particle-hole asymmetry is nearly perfectly mirrored while all other experimental parameters remain identical, see Figs. 3(a) and 3(b). As was the case for the spectra taken on the core, the noise on the tails [Figs. 3(c) and 3(d)] is reduced ($F^* < 1$) for the dominant resonance,

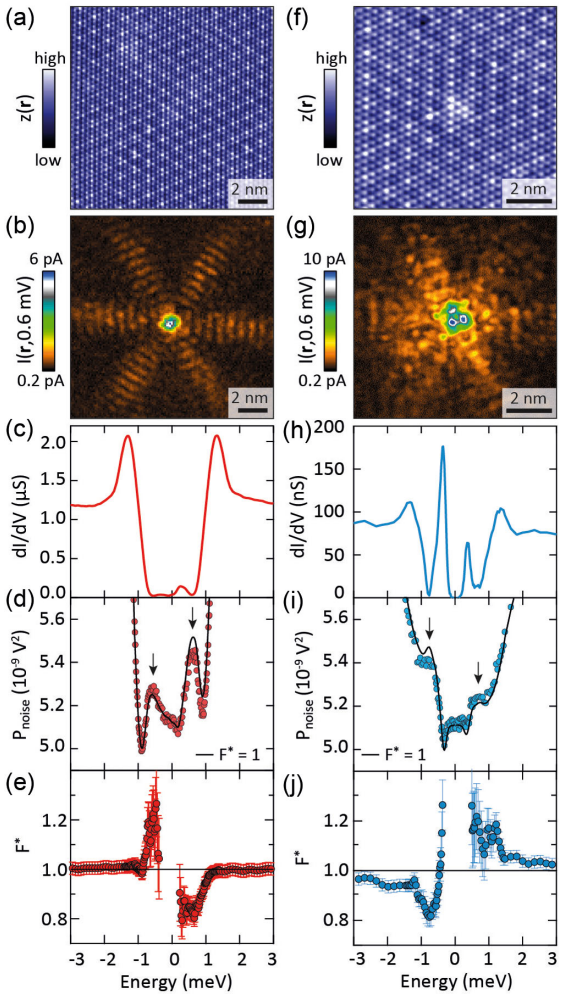

FIG. 2. (a) Atomically resolved constant current image of the Se surface of 2H-$NbSe_2$, $V = 4.2$ mV, $I = 100$ pA. (b) In-gap current recorded simultaneously with (a) showing a spatially extended YSR state generated by a subsurface impurity. (c) Tunneling spectrum taken at the core of the YSR and (d) simultaneously recorded current noise, $V = 3$ mV, $I = 3$ nA. The black line in (d) indicates $F^* = 1$: the noise from the YSR deviates at both positive and negative sample bias (arrows), as can be clearly seen in the effective Fano factor, F^*, in (e). Outside the gap, F^* converges to 1. (f)–(j) The same as (a)–(e) for a more compact, but relatively strong, YSR located elsewhere on the same sample [16]. $V = 4$ mV, $I = 100$ pA for (f),(g); $V = 6$ mV, $I = 400$ pA for (h)–(j).

and enhanced ($F^* > 1$) for the weaker resonance, and converges to Poissonian as soon as the current becomes dominated by the quasiparticles at the coherence peaks. We furthermore confirm that the noise depends linearly on the current as required for shot noise (see Fig. S5 [30]).

To gain more insight into our data, we calculate the tunneling current and current noise using a standard description of a classical YSR impurity, considering both single electron tunneling and Andreev processes [14]. The YSR density of states is approximated by a Lorentzian line shape centered at the YSR energy whose width is given by the intrinsic lifetime, $\tau = \hbar/\Lambda$, and the coupling of the YSR with the tip (details of the theory can be found in the Supplemental Material [30], Sec. 2). Among the theory parameters, the superconducting gap, Δ, the YSR energy, E_0, and the normal state conductance, G_N, can be directly obtained from the measured differential conductance spectra [e.g., Fig. 3(b)]. Furthermore, the coherence factors of

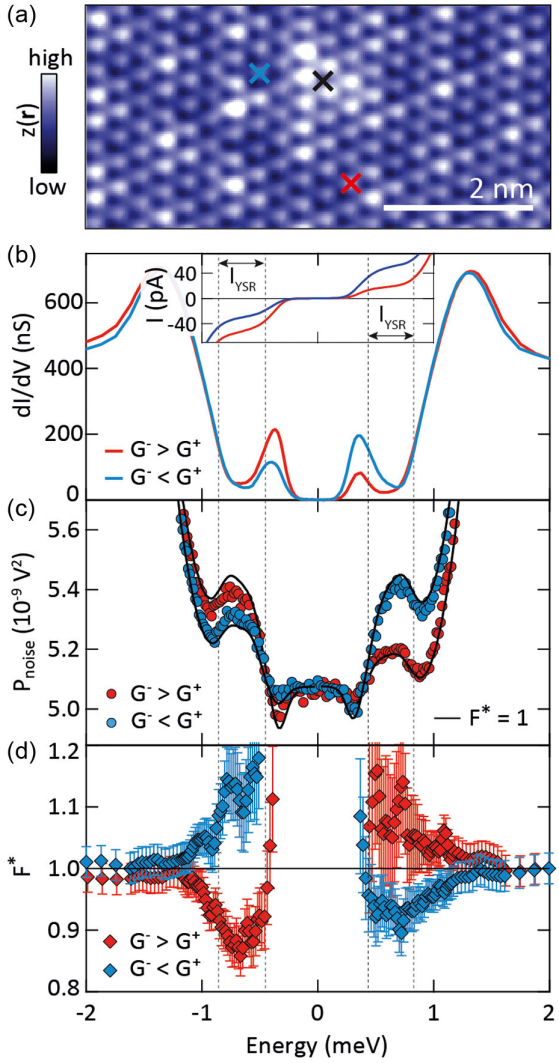

FIG. 3. (a) Constant current image of the same YSR state as Figs. 2(f)–2(j) ($V = 4$ mV, $I = 100$ pA). The black cross marks the location of the core. (b) Differential conductance $G = dI/dV$ on two tail locations [blue and red crosses in (a)] with opposite particle-hole asymmetry, $V = 4.2$ mV, $I = 1.5$ nA, $G^{\pm} = G(\pm E_0)$ with E_0 the YSR resonance energy. The inset shows the corresponding currents on the same energy scale, dashed lines indicate where the current is dominated by the YSR and is sufficiently large for noise measurements. (c) Current noise recorded simultaneously with (a), the black lines indicate $F^* = 1$. (d) Effective Fano factor, F^*, extracted from (c) showing clearly that the noise deviates from $F^* = 1$ where the current is dominated by the YSR.

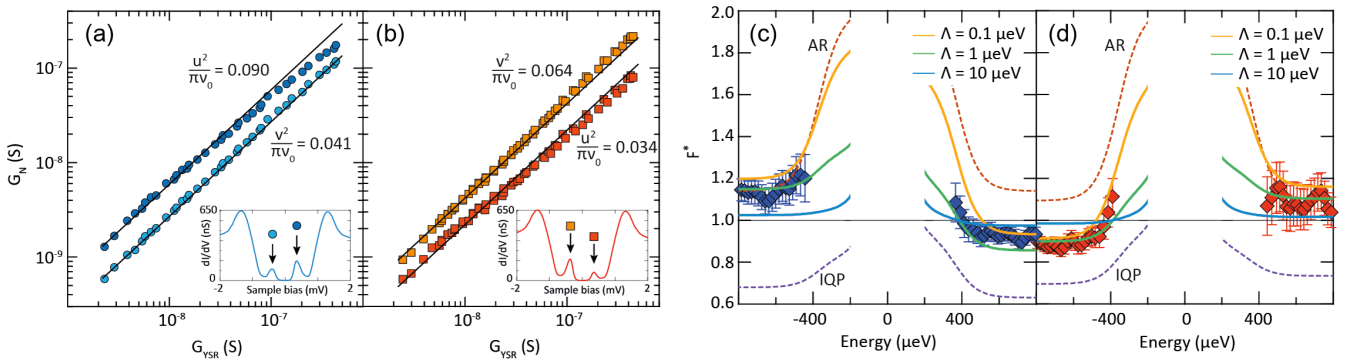

FIG. 4. YSR peak conductance (G_{YSR}) as function of normal state conductance (G_N) for the location of the blue (a) and red (b) spectrum of Fig. 3, reproduced here in the inset. A linear fit of the data taken at small conductance is used to extract u and v. Subgap F^* (symbols) for the blue (c) and red (d) spectrum of Fig. 3(d) and theoretical curves for three different values of Λ. Pure Andreev reflection (AR, $\Lambda = 0$ μeV) and pure inelastic quasiparticle tunneling (IQP, $\Lambda = 1$ μeV) are shown for comparison.

the electron and hole excitations of the YSR, u and v, can be extracted from the normal state conductance (G_N) dependence of the YSR conductance (G_{YSR}), see Figs. 4(a) and 4(b). Here, we fit the single electron tunneling dominated linear part at low conductance [14,15] to determine u and v. This enables us to calculate the noise with a single adjustable parameter, the intrinsic lifetime ($\hbar/\Lambda$), which is masked in the conductance by thermal broadening (see Ref. [30], Sec. 2F for a detailed theoretical study of temperature effects on noise in YSR states).

Figures 4(c) and 4(d) compare the noise data for energies where the tunneling current is carried exclusively by the YSR states (i.e., $|V| < 0.8$ mV) with theoretical curves for several values of Λ, showing quantitative agreement for $\Lambda \sim 1$ μeV, i.e., $\tau \sim 0.7$ ns, for both measured particle-hole asymmetries. We stress that for increasing values of Λ, meaning shorter relaxation times, single electron tunneling becomes less resonant (i.e., less ordered in time) and increasingly dominates the tunneling process. Indeed, for $\Lambda = 10$ μeV, the calculated noise is already nearly Poissonian ($F^* = 1$) for all voltages [see Figs. 4(c) and 4(d)], setting a lower limit on the relaxation time. For comparison, calculations using only Andreev reflection (AR) or only inelastic single electron processes (IQP) fail to reproduce the data for any Λ, as the former always has $F^* > 1$ for both polarities and the latter $F^* < 1$. We note that due to the reduced tunneling rate at voltages well below the resonance ($|E| \ll |E_0|$), the noise associated with IQP and AR tends to its Poissonian value of $F^* = 1$ and $F^* = 2$, respectively, as the curves for pure AR and IQP in Figs. 4(c) and 4(d) also show. This is because at these voltages, the time-ordering effect of resonant tunneling is suppressed. The upturn in F^* below the resonant energy for both polarities, does therefore not reflect a change in the ratio of AR and IQP, but is merely a result of the reduced current. A similar upturn in F^* seems to occur in the experiment, although the error bars are relatively large for these small currents. Lastly, whereas different values of Λ lead to very distinct signatures in the noise, the resonances in the corresponding differential conductance spectra are indistinguishable from one another as they only depend on u and v for $k_B T \gg \Lambda$.

Discussion.—The persistent enhancement of the noise for the smaller of the two YSR resonances in both experiment and theory directly proves the presence of Andreev processes, whereas the reduction in noise of the strong resonance results from a finite lifetime of the YSR. Which of the two processes is relatively more prominent for a given set of peaks naturally follows from the particle-hole asymmetry of the YSR. Since Andreev reflection requires an electron and hole to tunnel simultaneously, the particle and hole resonances for pure Andreev reflection will be identical. For particle-hole asymmetric peaks, the larger of the two resonances by default will have an inelastic contribution as the smaller resonance cannot accommodate Andreev reflection for all charge carriers in the big resonance. Conversely, the inelastic component is reduced, or even absent, for tunneling into the smaller of the two resonances at low junction resistances. The fact that we obtain qualitative agreement between theory and experiment for u and v extracted from the linear part of Figs. 4(a) and 4(b) while all noise data was recorded in the nonlinear part of Figs. 4(a) and 4(b) highlights the robustness of our results. We stress that although qualitatively still in agreement, the theoretical curves for the data taken on the cores [Figs. 2(e) and 2(j)] slightly deviate quantitatively (see Fig. S8 [30]), suggesting that tip and/or current induced effects may indeed play a role on the YSR core which is currently not included in the theory. Despite the less accurate fit, the noise recorded for both cores agrees best to the theory curves that use a lifetime similar to that obtained on the YSR tails. Although based on limited statistics due to the challenging nature of the experiment, the YSR lifetime in 2H-$NbSe_2$ therefore seems independent of the particular details of the magnetic impurity and the

measurement location for roughly equal YSR currents, which at subgap voltages constitute the only contribution to the current.

Furthermore, the subnanosecond value at ∼0.7 K we extract from the noise data is similar to that reported for Mn atoms on a Pb(111) surface [14], and not incompatible with the electron-phonon relaxation time in 2H-$NbSe_2$ [42]. Importantly, the energy scale of relaxation we obtain ($\Lambda = 1\ \mu$eV) is much smaller than the electron temperature, meaning that shot noise allows to determine the YSR lifetime even if the width of the resonance in the tunneling spectra is dominated by thermal broadening, or the current not thermally saturated [14]. More generally, we show that local measurements of fluctuations in the tunneling current provide direct evidence of the coherent transfer of charges equal to $2e$ through YSR states into the bulk, and enable one to probe energy scales and timescales inaccessible to conventional spectroscopy. Although experimentally challenging, we demonstrate the feasibility of using atomic scale shot noise to elucidate the transport dynamics through individual impurity resonances, which could in future studies be used to, e.g., distinguish trivial from nontrivial states.

We thank A. Mesaros, C. H. L. Quay, H. Aubin, J. Estève, and M. Civelli for insightful discussions. We would like to acknowledge funding from H2020 Marie Skłodowska-Curie Actions (Grant No. 659247) and the ANR (ANR-16-ACHN-0018-01 and ANR-19-CE47-0006).

*freek.massee@universite-paris-saclay.fr

[1] L. Yu, Acta Phys. Sin. **21**, 75 (1965).
[2] H. Shiba, Prog. Theor. Phys. **40**, 435 (1968).
[3] A. I. Rusinov, ZhETF Pis. Red. **9**, 146 (1969) [JETP Lett. **9**, 85 (1969)].
[4] A. V. Balatsky, I. Vekhter, and J.-X. Zhu, Rev. Mod. Phys. **78**, 373 (2006).
[5] A. Yazdani, B. A. Jones, C. P. Lutz, M. F. Crommie, and D. M. Eigler, Science **275**, 1767 (1997).
[6] S.-H. Ji, T. Zhang, Y.-S. Fu, X. Chen, X.-C. Ma, J. Li, W.-H. Duan, J.-F. Jia, and Q.-K. Xue, Phys. Rev. Lett. **100**, 226801 (2008).
[7] B. W. Heinrich, J. I. Pascual, and K. J. Franke, Prog. Surf. Sci. **93**, 1 (2018).
[8] G. C. Ménard, S. Guissart, Ch. Brun, S. Pons, V. S. Stolyarov, F. Debontridder, M. V. Leclerc, E. Janod, L. Cario, D. Roditchev, P. Simon, and T. Cren, Nat. Phys. **11**, 1013 (2015).
[9] S. Nadj-Perge, I. K. Drozdov, J. Li, H. Chen, S. Jeon, J. Seo, A. H. MacDonald, B. A. Bernevig, and A. Yazdani, Science **346**, 602 (2014).
[10] M. Ruby, F. Pientka, Y. Peng, F. von Oppen, B. W. Heinrich, and K. J. Franke, Phys. Rev. Lett. **115**, 197204 (2015).
[11] R. Pawlak, M. Kisiel, J. Klinovaja, T. Meier, S. Kawai, T. Glatzel, D. Loss, and E. Meyer, npj Quantum Inf. **2**, 16035 (2016).
[12] H. Kim, A. Palacio-Morales, T. Posske, L. Rózsa, K. Palotás, L. Szunyogh, M. Thorwart, and R. Wiesendanger, Sci. Adv. **4**, eaar5251 (2018).
[13] V. Perrin, M. Civelli, and P. Simon, Phys. Rev. B **104**, L121406 (2021).
[14] M. Ruby, F. Pientka, Y. Peng, F. von Oppen, B. W. Heinrich, and K. J. Franke, Phys. Rev. Lett. **115**, 087001 (2015).
[15] H. Huang, C. Padurariu, J. Senkpiel, R. Drost, A. Levy Yeyati, J. C. Cuevas, B. Kubala, J. Ankerhold, K. Kern, and C. R. Ast, Nat. Phys. **16**, 1227 (2020).
[16] The deviation from $F^* = 1$ outside the gap of Fig. 2(j) is likely due to the relatively large YSR peaks, meaning that the current noise outside the gap still carries a non-negligible YSR component.
[17] B. W. Heinrich, L. Braun, J. I. Pascual, and K. J. Franke, Nano Lett. **15**, 4024 (2015).
[18] M. Ormaza, P. Abufager, B. Verlhac, N. Bachellier, M.-L. Bocquet, N. Lorente, and L. Limot, Nat. Commun. **8**, 1974 (2017).
[19] L. Malavolti, M. Briganti, M. Hänze, G. Serrano, I. Cimatti, G. McMurtrie, E. Otero, P. Ohresser, F. Totti, M. Mannini, R. Sessoli, and S. Loth, Nano Lett. **18**, 7955 (2018).
[20] S. Kezilebieke, R. Žitko, M. Dvorak, T. Ojanen, and P. Liljeroth, Nano Lett. **19**, 4614 (2019).
[21] J. Figgins and D. K. Morr, Phys. Rev. Lett. **104**, 187202 (2010).
[22] B. Bryant, R. Toskovic, A. Ferrón, J. L. Lado, A. Spinelli, J. Fernández-Rossier, and A. F. Otte, Nano Lett. **15**, 6542 (2015).
[23] L. Farinacci, G. Ahmadi, M. Ruby, G. Reecht, B. W. Heinrich, C. Czekelius, F. von Oppen, and K. J. Franke, Phys. Rev. Lett. **125**, 256805 (2020).
[24] Ya. M. Blanter and M. Büttiker, Phys. Rep. **336**, 1 (2000).
[25] Y. Ronen, Y. Cohen, J.-H. Kang, A. Haim, M.-T. Rieder, M. Heiblum, D. Mahalu, and H. Shtrikman, Proc. Natl. Acad. Sci. U.S.A. **113**, 1743 (2016).
[26] T. Choi, T. Ihn, S. Schön, and K. Ensslin, Appl. Phys. Lett. **100**, 072110 (2012).
[27] X. Jehl, M. Sanquer, R. Calemczuk, and D. Mailly, Nature (London) **405**, 50 (2000).
[28] K. M. Bastiaans, D. Cho, D. Chatzopoulos, M. Leeuwenhoek, C. Koks, and M. P. Allan, Phys. Rev. B **100**, 104506 (2019).
[29] F. Massee, Q. Dong, A. Cavanna, Y. Jin, and M. Aprili, Rev. Sci. Instrum. **89**, 093708 (2018).
[30] See Supplemental Material at http://link.aps.org/supplemental/10.1103/PhysRevLett.128.247001, which includes Refs. [31–37], for more details on the experimental data and analysis, and for a detailed description of the theoretical study.
[31] Y. Noat, J. A. Silva-Guillén, T. Cren, V. Cherkez, C. Brun, S. Pons, F. Debontridder, D. Roditchev, W. Sacks, L. Cario, P. Ordejón, A. García, and E. Canadell, Phys. Rev. B **92**, 134510 (2015).
[32] S. Cocklin and D. K. Morr, Phys. Rev. B **110**, 125146 (2019).

[33] F. Pientka, L. I. Glazman, and F. von Oppen, Phys. Rev. B **88**, 155420 (2013).
[34] V. Kaladzhyan, C. Bena, and P. Simon, J. Phys. Condens. Matter **28**, 485701 (2016).
[35] M. Büttiker, Phys. Rev. B **33**, 3020 (1986).
[36] M. Büttiker, Phys. Rev. B **46**, 12485 (1992).
[37] D. Sánchez and R. López, Phys. Rev. B **71**, 035315 (2005).
[38] The spatial extent of the in-gap resonance as well as its particle-hole asymmetry depends on the type of magnetic impurity and its location [8,39,40].
[39] J. Senkpiel, C. Rubio-Verdú, M. Etzkorn, R. Drost, L. M. Schoop, S. Dambach, C. Padurariu, B. Kubala, J. Ankerhold, C. R. Ast, and K. Kern, Phys. Rev. B **100**, 014502 (2019).
[40] E. Liebhaber, S. Acero González, R. Baba, G. Reecht, B. W. Heinrich, S. Rohlf, K. Rossnagel, F. von Oppen, and K. J. Franke, Nano Lett. **20**, 339 (2020).
[41] S. Pradhan and J. Fransson, Phys. Rev. B **97**, 115409 (2018).
[42] A. Anikin, R. D. Schaller, G. P. Wiederrecht, E. R. Margine, I. I. Mazin, and G. Karapetrov, Phys. Rev. B **102**, 205139 (2020).